

# Time-Reversal symmetry breaking superconductivity in Dirac materials: application to $\text{Nb}_x\text{Bi}_2\text{Se}_3$

Luca Chirolli,<sup>1,\*</sup> Fernando de Juan,<sup>1,2</sup> and Francisco Guinea<sup>1,3</sup>

<sup>1</sup>*IMDEA-Nanoscience, Calle de Faraday 9, E-28049 Madrid, Spain*

<sup>2</sup>*Rudolf Peierls Centre for Theoretical Physics, Oxford, 1 Keble Road, OX1 3NP, United Kingdom*

<sup>3</sup>*Department of Physics and Astronomy, University of Manchester, Oxford Road, Manchester M13 9PL, United Kingdom*

We consider superconductivity in Dirac materials in the odd parity channel with pseudoscalar and vector order parameters that coexist due to their similar critical temperatures and study their coupled theory in the presence of magnetic dopants. We show that the coupling to the dopants favors the condensation of time-reversal symmetry breaking (TRSB) phases, characterized by a condensate magnetization and simultaneous ordering of the dopant moments. We find a rich phase diagram of TRSB phases characterized by peculiar bulk quasiparticles, with Weyl nodes and nodal lines, and distinctive surface properties. These findings may explain recent experiments on Nb-doped  $\text{Bi}_2\text{Se}_3$  that have reported on the possibility of TRSB superconductivity induced by Nb magnetic moments.

PACS numbers: 74.20.Rp, 74.20.Mn, 74.45.+c

*Introduction* – One of the most fascinating aspects of unconventional superconductivity is that the condensate can display spontaneous time reversal symmetry breaking (TRSB), hosting an intrinsic Cooper pair magnetization [1, 2]. This can occur only in multicomponent order parameter when the different components develop relative phases, as in the well known  $p + ip$  chiral state proposed for  $\text{Sr}_2\text{RuO}_4$  or the  $d + id$  state conjectured for some cuprate superconductors [1]. There is significant experimental evidence of TRSB superconductivity in these and other materials, obtained from muon spin rotation  $\mu\text{SR}$  such as in  $\text{UPt}_3$  [3] and  $\text{Sr}_2\text{RuO}_4$  [4], polar Kerr effect [5] and Josephson tunneling experiments, or from magnetization measurements as in Bi/Ni heterostructures [6–8]. The two-dimensional  $p + ip$  state in particular has attracted great interest as a topological superconductor with protected edge and vortex modes, of potential use in the field of quantum computation [9, 10]. In a three dimensional system chiral SC is also possible, allowing the realization of a Weyl superconductor with Majorana arcs on the surface [11–13], but realistic candidate materials for this superconducting state are lacking.

More recently, very compelling evidence for unconventional superconductivity has been reported in Dirac materials of the  $\text{Bi}_2\text{Se}_3$  family upon doping [16–18]. These studies were originally motivated by the prediction of intrinsically three dimensional, time-reversal invariant (TRI) topological superconductivity featuring protected Andreev surface states [22]. However, the rich phenomenology gathered so far reveals a more complicated picture. Superconductivity was first observed in  $\text{Cu}_x\text{Bi}_2\text{Se}_3$  [19–21], but evidence for the characteristic surface Andreev states has remained controversial [23–25]. Moreover, it was reported from nuclear magnetic resonance measurements [26] that there is rotation symmetry breaking in the superconducting state, which rather supports a different pairing state of nematic type [27].

Superconductivity was also reported in  $\text{Sr}_x\text{Bi}_2\text{Se}_3$  [28, 29] and in  $\text{Tl}_x\text{Bi}_2\text{Te}_3$  [30], but evidence for unconventional pairing is lacking. Most interestingly, superconductivity has also been reported in  $\text{Nb}_x\text{Bi}_2\text{Se}_3$  [14], where samples were shown to develop a spontaneous magnetization after the superconducting transition, while above  $T_c$  paramagnetic behavior is observed. It was claimed that the magnetization survives only at the surface in the Meissner state, and that it originates from Nb magnetic moments. A second torque magnetometry experiment on  $\text{Nb}_x\text{Bi}_2\text{Se}_3$  [15] shows clear signatures of rotation symmetry breaking that disappear at high fields.

This complicated phenomenology is perhaps best understood within the minimal model of a superconducting Dirac Hamiltonian with approximate rotation symmetry, where there are only three possible pairing channels: a conventional  $s$ -wave scalar, an odd-parity pseudoscalar, and a vector. In this model, the TRI topological superconductor is generated by the pseudoscalar order parameter  $\chi$ , while rotation symmetry breaking can only be produced by the vector order parameter  $\psi$ . TRSB superconductivity occurs when the relative phases between different order parameter components are non-zero. It has previously been shown that with only local interactions the phase with order parameter  $\chi$  always has a higher critical temperature than the one associated to  $\psi$ , precluding both rotational and time-reversal symmetry breaking and thus posing a theoretical challenge.

Motivated by the recent experiments, in this work we develop a theory of possible TRSB superconducting phases of doped Dirac Hamiltonians in the presence of magnetic impurities. We first show that when further neighbor electron-electron interactions are included, the critical temperature of  $\psi$  raises and can become comparable to that of  $\chi$ . This leads us to consider a theory of fourth order coupling between  $\chi$  and  $\psi$  where, in absence of magnetic impurities, both order parameters condense

in a TRI nematic phase. We show that the presence of magnetic impurities, which would otherwise be paramagnetic, favors the condensation of TRSB phases and the consequent ordering of the magnetic impurities. Depending on microscopic parameters, we find three TRSB phases that differ in the way rotation and gauge symmetry are broken and can be distinguished by their bulk spectrum, which may be gapped or feature Weyl nodes or nodal lines.

*Superconductivity in Dirac materials* – We now consider the possible superconducting instabilities of Dirac Hamiltonians. To make contact with previous work, we start with the Hamiltonian commonly employed to describe Bi<sub>2</sub>Se<sub>3</sub> [22]

$$\mathcal{H}_0 = m\sigma_x + v\sigma_z(k_x s_y - k_y s_x) + v_z k_z \sigma_y, \quad (1)$$

where  $s_i$  are spin Pauli matrices and  $\sigma_i$  are Pauli matrices for  $p_z$ -orbitals in the top and bottom layer of the quintuple layer QL Bi<sub>2</sub>Se<sub>3</sub> structure,  $v$  is the Fermi velocity,  $m$  the insulating mass. The time reversal operator is  $\mathcal{T} = i s_y K$  with  $K$  complex conjugation and commutes with  $\mathcal{H}_0$ . When  $v_z = v$ , this Hamiltonian is a particular realization of the isotropic Dirac Hamiltonian of the form

$$\mathcal{H}_0 = \gamma_0 m + v \gamma_0 \gamma_i k_i \quad (2)$$

where the Euclidean gamma matrices  $\gamma_\mu = (\gamma_0, \gamma_i)$  satisfy  $[\gamma_\mu, \gamma_\nu]_+ = \mathcal{I}_{\mu\nu}$  and are given by  $\gamma_\mu = (\sigma_x, -\sigma_y s_y, \sigma_y s_x, \sigma_z)$ . In this work we will preferentially use the general Dirac matrices to emphasize the structure of the rotation group:  $\gamma_i$  transforms as a vector,  $\gamma_0$  as a scalar, and the matrix  $\gamma_5 \equiv \gamma_0 \gamma_1 \gamma_2 \gamma_3$  as a pseudoscalar.

To classify the possible pairing channels, we introduce the Nambu spinor  $\Psi_{\mathbf{k}} = (\mathbf{c}_{\mathbf{k}}^\dagger, i s_y \mathbf{c}_{-\mathbf{k}})^T$ , with  $\mathbf{c}_{\mathbf{k}}$  fermionic annihilation operators of  $\mathcal{H}_0$ , and consider the Bogolyubov-deGennes Hamiltonian  $\hat{H} = \frac{1}{2} \int d\mathbf{k} \Psi_{\mathbf{k}}^\dagger \mathcal{H}_{\mathbf{k}} \Psi_{\mathbf{k}}$ , with

$$\mathcal{H}_{\mathbf{k}} = (\mathcal{H}_0(\mathbf{k}) - \mu)\tau_z + \Delta_{\mathbf{k}}\tau_+ + \Delta_{\mathbf{k}}^\dagger\tau_-, \quad (3)$$

where  $\mu$  is the chemical potential,  $\Delta_{\mathbf{k}}$  stands for generic momentum-dependent  $4 \times 4$  pairing matrices and  $\tau_i$  Pauli matrices act in the particle-hole space. The Nambu construction imposes the charge conjugation symmetry  $\mathcal{C}$  implemented as  $U_{\mathcal{C}}\mathcal{H}(-\mathbf{k})^*U_{\mathcal{C}}^\dagger = -\mathcal{H}(\mathbf{k})$ , with  $U_{\mathcal{C}} = s_y \tau_y$ , which amounts to the restriction  $s_y \Delta^*(-\mathbf{k})s_y = \Delta(\mathbf{k})$ . If pairing is momentum independent [22, 31], only six possible matrices in the Dirac algebra satisfy this constraint: the two even-parity scalars  $I$  and  $\gamma^0$ , the pseudo-scalar  $\gamma^5$  and the vector  $\gamma^i$ , which are both odd under parity. Disregarding the even-parity scalars, the pairing matrix takes the form  $\Delta = \chi\gamma^5 + \boldsymbol{\psi} \cdot \boldsymbol{\gamma}$ . For the specific model of Bi<sub>2</sub>Se<sub>3</sub>, it was concluded that the local interorbital interaction  $V$  can give rise to pairing in both of these channels, but the critical temperatures of the two channels satisfy  $T_\chi \gg T_\psi$ , [22]. Such a difference in critical temperatures

makes it unlikely that the system would condense in the vector channel, in conflict with experiments that observe both rotational and time-reversal symmetry breaking.

We suggest that this problem can be solved by considering momentum-dependent interactions. To be specific, we consider nearest-neighbor corrections to the inter-orbital interactions in Bi<sub>2</sub>Se<sub>3</sub> in the form of a two-body density-density interaction

$$H_{\text{int}} = -\frac{1}{2} \sum_{i \neq j} \int d\mathbf{r} d\mathbf{r}' V(\mathbf{r} - \mathbf{r}') n_i(\mathbf{r}) n_j(\mathbf{r}'), \quad (4)$$

where  $n_i(\mathbf{r}) = \sum_{is} n_{is}(\mathbf{r})$  is the local density in orbital  $i$  comprising both spin projection  $s$ . Expanding the interaction potential at lowest order in  $\mathbf{q} = \mathbf{k} - \mathbf{k}'$  one has

$$V(\mathbf{k}, \mathbf{k}') = V(1 + a^2 \mathbf{k} \cdot \mathbf{k}'), \quad (5)$$

with  $a$  a length scale on order of the lattice constant. In order to decouple the additional momentum-dependent interaction term we need to consider the other ten matrices in the Dirac algebra [32]. In particular, we note that that pairing matrix  $\gamma^5 \gamma^i k^j \epsilon_{ijk}$  is also a vector, and it modifies the gap matrix as

$$\Delta_{\mathbf{k}} = \chi\gamma^5 + \boldsymbol{\psi} \cdot (\boldsymbol{\gamma} - ia\gamma^5 \boldsymbol{\gamma} \times \mathbf{k}). \quad (6)$$

It is instructive to project the  $4 \times 4$  Dirac matrices into the  $2 \times 2$  space of the Kramers degenerate conduction band states relevant to pairing [33]. If we define Pauli matrices  $\tilde{s}_i$  for this space, the gap matrix takes the form  $\Delta_{\mathbf{k}} = \chi \tilde{\mathbf{k}} \cdot \tilde{\mathbf{s}} + \boldsymbol{\psi} \times \tilde{\mathbf{k}} \cdot \tilde{\mathbf{s}}(1 + \mu a/v)$ , with  $\tilde{\mathbf{k}} = v\mathbf{k}/\mu$ . Thus, while seemingly of higher order in the Dirac Hamiltonian, the correction term is actually of the same order when projected to the Fermi surface. The momentum dependence of the pairing interaction affects only the vector channel and it raises its critical temperature  $T_\chi$ , which becomes comparable to  $T_\chi$  [32].

*Ginzburg-Landau free energy* – We now consider superconductivity at the level of the Ginzburg-Landau free energy. The pseudoscalar order parameter free energy is written as

$$F_\chi = a_1 |\chi|^2 + b_1 |\chi|^4 \quad (7)$$

and condensation of  $\chi$  takes place when  $a_1(T_\chi) = 0$ . For the vector order parameter  $\boldsymbol{\psi}$ , symmetry dictates that the form of the free energy be [34, 35]

$$F_\psi = a_2 |\boldsymbol{\psi}|^2 + b_2 |\boldsymbol{\psi}|^4 + b'_2 |\boldsymbol{\psi} \times \boldsymbol{\psi}^*|^2. \quad (8)$$

The vector representation admits two possible superconducting states: a nematic state  $\boldsymbol{\psi} \propto (1, 0, 0)$  which is time-reversal invariant, and a chiral TRSB state  $\boldsymbol{\psi} \propto (1, \pm i, 0)$  [27, 36]. The sign of the coupling  $b'_2$  determines whether the vector representation chooses the nematic (for  $b'_2 > 0$ ) or the chiral state (for  $b'_2 < 0$ ). Since at

second order no coupling is allowed by symmetry between  $\chi$  and  $\psi$ , the condensation of  $\psi$  takes place when  $a_2(T_\psi) = 0$ . However, our previous argument suggesting that  $a_1 \sim a_2$  [32] and  $T_\chi \sim T_\psi$  require that we study a coupled theory beyond second order where both order parameters may coexist. At fourth order the coupling term in the GL free energy reads,

$$F_{\psi,\chi} = d_1 |\chi|^2 |\psi|^2 + d_2 |\chi^* \psi - \chi \psi^*|^2, \quad (9)$$

and the total free energy is

$$F = F_\chi + F_\psi + F_{\chi,\psi}. \quad (10)$$

In the weak coupling regime with  $a_1 \sim a_2$  both order parameters acquire a finite value.

The possible TRSB phases that arise from this free energy are characterized by a magnetization of the condensate, which arises due to the spin triplet state of the Cooper pairs. By symmetry, the magnetization must be built with gauge invariant combinations of order parameters and have the correct symmetry properties of a spin, i.e. a  $\mathcal{T}$ -odd pseudo-vector (even under inversion, odd under mirror). Since  $\psi$  is a vector and  $\chi$  a pseudo-scalar, the following combinations satisfy the symmetry requirements,

$$\Sigma_1 = \chi \psi^* - \chi^* \psi, \quad \Sigma_2 = \psi \times \psi^*.$$

Note that  $\Sigma_1$  cannot be built with a standard  $s$ -wave order parameter because the combination would not be a pseudovector. These two pseudovectors are orthogonal and appear quadratically in the GL Eqs. (8, 9). The condensation of either of these pseudovectors breaks the rotation and gauge symmetry of the free energy in a certain way which distinguishes the different phases. In a TRSB phase  $\Sigma_1$  is always non-zero, whereas the value of  $\Sigma_2$  depends on the phase and its symmetries.

The phase diagram of the GL free energy Eq. (10) depends on the sign of the interaction parameters  $b'_2$  and  $d_2$ , and it is possible to label the different phases that can occur by the value of  $\Sigma_1$  and  $\Sigma_2$  and the symmetries that they preserve. For  $d_2, b'_2 > 0$  one has  $\Sigma_1 = \Sigma_2 = 0$  and the system is in the TRI nematic phase, with rotation symmetry about the nematic director. When  $d_2 < 0$  and  $b'_2 > 0$  one has  $\Sigma_1 \neq 0$  and  $\Sigma_2 = 0$ , and the system is invariant under rotations about  $\Sigma_1$ . We name this phase TRSB 1. When  $d_2, b'_2 < 0$  one has  $\Sigma_2 \neq 0$ , and the system is in the chiral phase, with  $\psi \propto (1, i, 0)$ . In this case the system is invariant under rotations around  $\Sigma_2$  combined with a gauge transformation [32]. Finally, when  $d_2 > 0$  and  $b'_2 < 0$  one has  $\Sigma_2 \neq 0$ , but  $\psi$  is not in the purely chiral state, but rather in a hybrid solution [32] which preserves no symmetry. We name this phase TRSB 2.

The phase diagram as a function of  $b'_2$  and  $d_2$  is schematically depicted in Fig. 1. Microscopic calculations [27, 32, 36] show that for an isotropic model

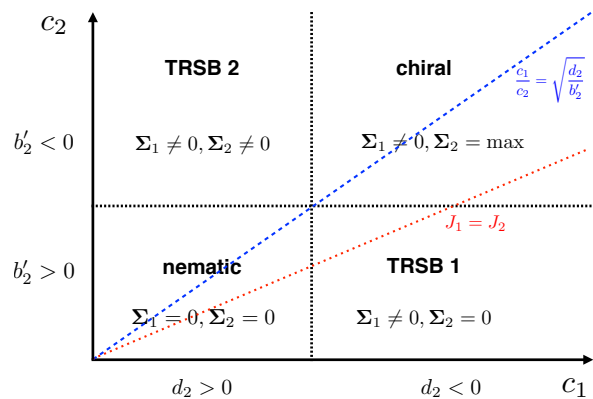


FIG. 1: Phase diagram of superconductivity involving the pseudo-scalar and the vector order parameters coupled to the dopants magnetization. The four possible phases can be obtained by properly tuning the couplings  $J_1$  and  $J_2$ .

$b'_2, d_2 > 0$ , so that no TRSB phase may arise in the system. We show next that a sufficiently strong coupling to magnetic dopants can renormalize the coefficient  $b'_2$  and  $d_2$  and effectively change their sign.

*Coupling to dopant magnetization* – Next we consider the presence of random magnetic moments in the sample, described by an average magnetization  $\mathbf{M}$ . At the Landau theory level, both  $\Sigma_1$  and  $\Sigma_2$  can couple linearly to this magnetization which is also a  $\mathcal{T}$ -odd pseudo-vector

$$F_{\chi,\psi,M} = i\mathbf{M} \cdot [c_1(\chi\psi^* - \chi^*\psi) + c_2\psi \times \psi^*]. \quad (11)$$

By appropriately aligning  $\mathbf{M}$ , we see that the system may lower its energy by condensing in a TRSB phase with finite condensate magnetizations.

Neglecting interactions between the magnetic moments, the full free energy at second order in  $\mathbf{M}$  including its coupling to the superconducting order parameters reads

$$F = a_3 |\mathbf{M}|^2 + F_\chi + F_\psi + F_{\chi,\psi} + F_{\chi,\psi,M}. \quad (12)$$

Since the dopants are paramagnetic above  $T_c$ , we assume  $a_3 > 0$ . The mean-field solution for  $\mathbf{M}$  can be found by minimizing the free energy with respect to  $\mathbf{M}$ , and one finds  $\mathbf{M} = -i\frac{c_1}{2a_3}\Sigma_1 - i\frac{c_2}{2a_3}\Sigma_2$ . It becomes clear that a non-zero magnetization  $\mathbf{M}$  arises if the system is in a TRSB phase, despite the fact that the dopants being initially paramagnetic. By substituting the saddle point value of the magnetization the free energy of the scalar and vector order parameter reads exactly as Eq. (10) with the modified parameters

$$d_2 \rightarrow d_2 - \frac{c_1^2}{4a_3}, \quad b'_2 \rightarrow b'_2 - \frac{c_2^2}{4a_3}. \quad (13)$$

We see that both the coefficients  $b'_2$  and  $d_2$  are renormalized by the coupling to the magnetic order, that favors

TRSB phases, and by varying  $c_1$  and  $c_2$  one can span the entire phase diagram in Fig. 1.

*Microscopic coupling* – The coupling to an external magnetization Eq. (11) and the resulting phase diagram is generic of a SO(3) invariant theory. With this symmetry, the only microscopic coupling allowed between magnetic impurities described by  $\mathbf{M}$  and the electronic degrees of freedom must be written in terms of the spin pseudovectors  $\mathbf{S}_{\parallel} \equiv (s_x, s_y, \sigma_x s_z)$  and  $\mathbf{S}_{\perp} \equiv (\sigma_x s_x, \sigma_x s_y, s_z)$  [32]. This general coupling is

$$H_Z = J_1 \mathbf{M} \cdot \mathbf{S}_{\parallel} + J_2 \mathbf{M} \cdot \mathbf{S}_{\perp}. \quad (14)$$

The coefficients  $c_1$  and  $c_2$  can be derived microscopically from this coupling, which implies a constraint relating them to the coupling constants  $J_1$  and  $J_2$ ,  $c_1(J_1 m/\mu + J_2) = 2c_2(J_1 + J_2 m/\mu)$  [32]. All phases in the phase diagram in Fig. 1 can therefore be realized by properly tuning  $J_1$ ,  $J_2$ , and  $m/\mu$ .

In the  $\text{Bi}_2\text{Se}_3$  model, the SO(3) symmetry is only approximate and it breaks down to the lattice point group  $D_{3d}$  when anisotropy corrections are included. In this case [22], the vector representation  $\psi = (\psi_x, \psi_y, \psi_z)$  splits into a two-component  $E_u \sim (-\psi_y, \psi_x)$  and one-component  $A_{2u} \sim \psi_z$  representations with different coefficients in the GL free energy, Eq. (8). The pseudoscalar  $\chi$  corresponds to the  $A_{1u}$  representation. A microscopic coupling between the magnetic moments and the physical spin  $\mathbf{s} = (s_x, s_y, s_z)$  of the electrons in  $\text{Bi}_2\text{Se}_3$  can be written in terms of a Zeeman coupling

$$H_Z = -J(s_x M_x + s_y M_y) - J_z s_z M_z, \quad (15)$$

with  $J \neq J_z$  anisotropic Zeeman coupling constants. This term breaks the SO(3) symmetry group generated by the Dirac algebra even in the case  $J = J_z$ , because the physical spin is built by mixing of the two pseudovectors  $\mathbf{S}_{\parallel}$  and  $\mathbf{S}_{\perp}$ . Nonetheless, the resulting phase diagram remains qualitatively very similar to the SO(3) invariant one [32]. The presence of the magnetic dopants induces the condensation of a TRSB phase and, at the same time, the ordering and alignment of the magnetic moments of the dopants with the magnetization of the condensate.

*Gap structure* – The value of the gap on the Fermi surface of the different superconducting phases depends on the relative strength of the two order parameters. When  $\chi$  dominates all the phases are fully gapped. When  $\psi$  dominates each phase has its own gap structure. In the nematic case the gap has Dirac nodes along the nematic direction for  $\chi = 0$ . These nodes can be gapped by any perturbation such as a small  $\chi$  or by the inclusion of in-plane hexagonal warping terms [27], so that in general the phase is fully gapped. In the TRSB 1 phase the order parameters may be taken as  $\psi = \psi_0(1, 0, 0)$  and  $\chi = \chi_0 e^{i\gamma}$  and that the Dirac nodes for  $\chi = 0$  can be shown to become circular nodal lines defined by  $\sin \theta = \pm \chi_0/\psi_0$ , with  $\theta$  the polar angle with respect to  $\Sigma_1$ . Nodal lines

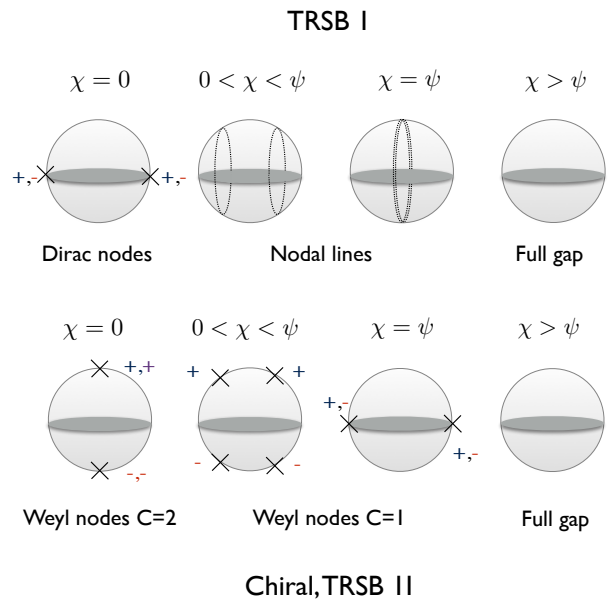


FIG. 2: Schematics of the gap structure on the Fermi surface: TRSB 1 has Dirac nodes that evolve in nodal line for  $\chi > 0$ . TRSB 2 and the chiral phase have Weyl points with  $C = 2$  that split in two  $C = 1$  upon switching  $\chi$ . The phases are fully gapped for  $\chi > \psi$ .

of the north and south hemisphere join for  $\chi = \psi$  and become gapped for  $\chi > \psi$  (see Fig. 2). This phase can be distinguished by its DOS  $\rho(\epsilon) \propto \epsilon$  [37]. In the chiral and the TRSB 2 phase one has a Weyl superconductor [11–13, 36]. For  $\chi = 0$  one has Weyl nodes of topological charge  $C = \pm 2$  on the north and south pole along the direction of  $\Sigma_2$  [38]. Weyl points cannot be gapped unless nodes of opposite charge  $C$  are brought to coincide. Upon switching on  $\chi$  these nodes are split into two Weyl nodes of  $C = 1$  at a finite polar angle and by increasing  $\chi$  they move towards the equator where they meet with the nodes from the south hemisphere and eventually gap out for  $\chi > \psi$  (see Fig. 2). Note that while the DOS is linear in energy when  $\chi = 0$ ,  $\rho_{C=2}(\epsilon) \propto \epsilon$ , it becomes quadratic for finite  $\chi$ ,  $\rho_{C=1}(\epsilon) \propto \epsilon^2$ , [39]. These predictions could be experimentally confirmed by STM or specific heat measurements. On the surface of Weyl superconductor there are Majorana arcs of different kinds [38], while in the gapped phases the topologically protected surface Andreev states associated to  $\chi$  are now gapped in the surfaces perpendicular to  $\Sigma_1$ .

*Conclusions* – In summary, we have shown that the presence of local magnetic moments can enhance the TRSB superconducting instabilities of doped Dirac fermions, with the particular phase realized depending on the coupling between the pseudoscalar and the vector order parameters. The different phases predicted have characteristic bulk and surface excitations that could be probed in current materials hosting Dirac fermions such as the doped  $\text{Bi}_2\text{Se}_3$  family.

*Note* – During the preparation of this manuscript, we became aware of Ref. [40] which presents similar results to those obtained in this work for the chiral phase. The coupling to the pseudoscalar is however not considered.

*Acknowledgements* – The authors acknowledge useful discussions with Irina Grigorieva. The authors acknowledge funding from the European Union’s Seventh Framework Programme (FP7/2007-2013) through the ERC Advanced Grant NOVGRAPHENE through grant agreement Nr. 290846 (L. C., F. J. and F. G.), from the Marie Curie Programme under EC Grant agreement No. 705968 (F. J.) and from the European Commission under the Graphene Flagship, contract CNECTICT-604391 (F. G.).

- [36] J. W. F. Venderbos, *et al.*, arXiv: 1512.04554 (2015).
- [37] M. Phillips and V. Aji, Phys. Rev. B **90**, 115111(2014).
- [38] V. Kozii, J. W. F. Venderbos, and L. Fu, arXiv:1607.08243 (2016).
- [39] C. Fang, M. J. Gilbert, X. Dai, B. A. Bernevig, Phys. Rev. Lett. **108**, 266802 (2012).
- [40] N. F. Q. Yuan, W.-Y. He, K. T. Law, arXiv:1608.05825 (2016).

---

\* luca.chirolli@imdea.org

- [1] M. Sigrist and K. Ueda, Rev. Mod. Phys. **63**, 239 (1991).
- [2] Y. Maeno, *et al.*, Nature **372**, 532 (1994).
- [3] G. M. Luke, *et al.*, Phys. Rev. Lett. **71**, 1466 (1993).
- [4] G. M. Luke, *et al.*, Nature **394**, 558 (1998).
- [5] A. Kapitulnik *et al.*, New J. Phys. **11**, 055 060 (2009).
- [6] P. LeClair *et al.*, Phys. Rev. Lett. **94**, 037006 (2005).
- [7] X.-X. Gong, *et al.*, arXiv:1504.04232 (2015).
- [8] X.-X. Gong, *et al.*, arXiv:1609.08538 (2016).
- [9] C. Nayak, *et al.*, Rev. Mod. Phys. **80**, 1083 (2008).
- [10] X.-L. Qi and S.-C. Zhang Rev. Mod. Phys. **83**, 1057 (2011).
- [11] T. Meng and L. Balents, Phys. Rev. B **86**, 054504 (2012).
- [12] J. D. Sau and S. Tewari, Phys. Rev. B **86**, 104509 (2012).
- [13] S. A. Yang, *et al.*, Phys. Rev. Lett. **113**, 046401 (2014).
- [14] Qiu *et al.*, arXiv:1512.03519, (2015).
- [15] Asaba *et al.*, arXiv:1603.04040 (2016).
- [16] H. Zhang *et al.*, Nature Physics **5**, 438 (2009).
- [17] M. Z. Hasan and C. L. Kane, Rev. Mod. Phys. **82**, 3045 (2010).
- [18] X.-L. Qi and S.-C. Zhang, Rev. Mod. Phys. **83**, 1057 (2011).
- [19] Y. S. Hor *et al.*, Phys. Rev. Lett. **104**, 057001 (2010).
- [20] L. A. Wray, *et al.*, Nature Physics **6**, 855 (2010).
- [21] M. Kriener *et al.*, Phys. Rev. Lett. **106**, 127004 (2011).
- [22] L. Fu, E. Berg, Phys. Rev. Lett. **105**, 097001 (2010).
- [23] S. Sasaki *et al.*, Phys. Rev. Lett. **107**, 217001 (2011).
- [24] N. Levy *et al.*, Phys. Rev. Lett. **110**, 117001 (2013).
- [25] H. Peng, *et al.*, Phys. Rev. B **88**, 024515 (2013).
- [26] Matano *et al.*, Nat. Phys. **12**, 852 (2016)
- [27] Liang Fu, Phys. Rev. B **90**, 100509(R) (2014).
- [28] Shruti *et al.*, Phys. Rev. B **92**, 020506 (2015).
- [29] Liu *et al.*, J. Amer. Chem. Soc. **137**, 10512 (2015).
- [30] Wang *et al.* Chem. Mater. **28**, 779 (2016).
- [31] T. Hashimoto *et al.*, Phys. Rev. B **94**, 014510 (2016).
- [32] See Supplementary Material for details on the Dirac matrices, the microscopic theory for Bi<sub>2</sub>Se<sub>3</sub>, the minimization of Landau free energies, and the gap structure on the Fermi surface.
- [33] L. Fu, Phys. Rev. Lett. **115**, 026401 (2015).
- [34] K. Ueda and T. M. Rice, Phys. Rev. B **31**, 7114 (1985).
- [35] A. Knigavko and B. Rosenstein, Phys. Rev. Lett. **82**, 1261 (1999).

### Character on the Fermi surface: Dirac nodes, Weyl nodes, Majorana nodes

The four different phases that appear in the phase diagram of the pseudoscalar and vector order parameters coupled to a magnetization order parameter have a peculiar character on the Fermi surface. By writing the gap matrix as  $\Delta = \mathbf{d}_\mathbf{k} \cdot \mathbf{s}$ , the character on the Fermi surface can be addressed by studying the bulk spectrum

$$E_\pm(\mathbf{k}) = \sqrt{(\epsilon_\mathbf{k} - \mu)^2 + |\mathbf{d}_\mathbf{k}|^2 \pm |\mathbf{d}_\mathbf{k} \times \mathbf{d}_\mathbf{k}^*|}, \quad (16)$$

on the Fermi surface  $\epsilon_\mathbf{k} = \mu$ . With the vector  $\mathbf{d}_\mathbf{k} = \chi\mathbf{k} + \boldsymbol{\psi} \times \mathbf{k}$  one can write the gap in terms of the condensate magnetization  $\boldsymbol{\Sigma}_1$  and  $\boldsymbol{\Sigma}_2$  as

$$\Delta_\pm(\mathbf{k}) = \sqrt{(|\chi|^2 + |\boldsymbol{\psi}|^2)k^2 - |\boldsymbol{\psi} \cdot \mathbf{k}|^2 \pm k\sqrt{|\boldsymbol{\Sigma}_1|^2 k^2 - |\boldsymbol{\Sigma}_1 \cdot \mathbf{k}|^2 + |\boldsymbol{\Sigma}_2 \cdot \mathbf{k}|^2}}, \quad (17)$$

with  $\mathbf{k}$  on the Fermi surface,  $k = 1$ . For  $\boldsymbol{\psi} = 0$  the phase is fully gapped, with  $\Delta_\pm = |\chi|$

#### Nematic state

In the nematic phase one has  $\chi$  and  $\boldsymbol{\psi}$  both real, so that  $\boldsymbol{\Sigma}_1 = \boldsymbol{\Sigma}_2 = 0$ , and the gap reads

$$\Delta_\pm^{\text{nem}}(\mathbf{k}) = \sqrt{|\chi|^2 + |\boldsymbol{\psi}|^2 - |\boldsymbol{\psi} \cdot \hat{\mathbf{k}}|^2}, \quad (18)$$

so that the phase is fully gapped as long as  $\chi \neq 0$ , whereas for  $\chi = 0$  it has a two double degenerate nodes for  $\hat{\mathbf{k}} \parallel \boldsymbol{\psi}$ . These nodes represent Dirac points and can be gapped by hexagonal warping [27].

#### Chiral state

In the chiral phase one has  $\chi$  real and  $\boldsymbol{\psi} = \psi(\mathbf{u} + i\mathbf{v})$ , with  $\mathbf{u}$  and  $\mathbf{v}$  orthogonal unit vectors. Let us first consider the case  $\chi = 0$ . The gap then reads

$$\Delta_\pm(\mathbf{k}) = \sqrt{|\boldsymbol{\psi}|^2 - |\boldsymbol{\psi} \cdot \mathbf{k}|^2 \pm |\boldsymbol{\Sigma}_2 \cdot \mathbf{k}|}, \quad (19)$$

It is clear that only the gap  $\Delta_-$  can be zero on a given point  $(\theta, \phi)$  of the Fermi surface. Due to  $\text{SO}(3)$  symmetry we can choose for simplicity  $\boldsymbol{\psi} = \psi(1, i, 0)$ , so that by writing  $\hat{\mathbf{k}} = (\sin\theta \cos\phi, \sin\theta \sin\phi, \cos\theta)$  the gap reads

$$\Delta_\pm^{\text{chi}}(\mathbf{k}) \propto \psi(1 \pm |\cos\theta|). \quad (20)$$

One has a node on the north pole  $\theta = 0$  and a node on the south pole  $\theta = \pi$  on the Fermi sphere. Each node represents a Weyl point with topological charge  $C = \pm 2$ , with  $C = +2$  at the north pole and  $C = -2$  at the south pole. These nodes cannot be gapped unless nodes with opposite topological charge are brought into contact.

We can see this in more details by expanding the Hamiltonian in the reduced subspace of the conduction band for small momentum  $\mathbf{q}$  around the the nodal points. For  $\chi = 0$  these are the north and south pole  $\mathbf{k}_F^\pm = (0, 0, \pm k_F)$ , and the Hamiltonian reads

$$H_{\pm, \mathbf{q}}^{\text{chi}} = \begin{bmatrix} \pm v_F q_z & 0 & -i\psi q_+ & \pm 2i\psi k_F \\ 0 & \pm v_F q_z & 0 & i\psi q_+ \\ i\psi q_- & 0 & \mp v_F q_z & 0 \\ \mp 2i\psi k_F & -i\psi q_- & 0 & \mp v_F q_z \end{bmatrix}, \quad (21)$$

where  $q_\pm = q_x \pm iq_y$ . We see that the Hamiltonian splits into two Weyl sub-blocks coupled by a mass term  $m = 2\psi k_F$  and the resulting eigenvalues give rise to two gapped bands at  $\pm m$  and two gapless bands. Projecting onto the gapless states we find

$$h_{\pm, \mathbf{q}}^{\text{chi}} = \pm \left[ v_F q_z \sigma_z - \frac{\psi^2}{m} (iq_+^2 \sigma_+ - iq_-^2 \sigma_-) \right], \quad (22)$$

that is linearly dispersing along  $q_z$  but quadratically dispersing along  $q_x$  and  $q_y$ . One can show that the topological charge of these band crossing is  $C = \pm 2$ .

When  $\chi \neq 0$  the gap reads

$$\Delta_{\pm}^{\text{chi}}(\mathbf{k}) \propto \psi \sqrt{(\chi/\psi)^2 + 1 + \cos^2(\theta) \pm 2\sqrt{\cos^2(\theta)((\chi/\psi)^2 + 1) + (\chi/\psi)^2 \cos^2(\phi) \sin^2(\theta)}}. \quad (23)$$

One can look for nodal solutions of  $\Delta_{-}$ , that reduces to solve  $\cos^2 \theta_W = 1 - (\chi/\psi)^2 e^{\pm 2i\phi}$ , and find there exist Weyl nodes with topological charge  $|C| = 1$  for  $0 < \chi < \psi$  only for  $\phi = 0, \pi$ . The Weyl node with topological charge 2 is separated into two Weyl nodes with topological charge  $C = 1$  at finite angles  $\pm\theta_W$  in the  $x, z$  plane ( $\phi = 0$ ), and analogously for the nodes at the south pole. The quadratic crossing splits into two linear crossing with  $C = 1$  in the north hemisphere and two linear crossing with  $C = -1$  in the south hemisphere. It follows that by increasing  $\chi$  one moves the Weyl nodes toward the equator and for  $\chi = \psi$  one has that Weyl nodes of opposite charge are brought into contact and split, so that for  $\chi > \psi$  the system is fully gapped.

In the plane  $\phi = 0$  the nodes are located at  $\sin \theta_W = \pm\chi/\psi$ . We expand the Hamiltonian around the point  $\hat{\mathbf{k}}_F = (\sin \theta_W, 0, \cos \theta_W)$ , and define radial and tangential momentum  $\mathbf{q} = (q_{\parallel,x}, q_{\parallel,y}, q_{\perp})$ ,

#### TRSB 1 state

In the TRSB phase 1 characterized by  $\Sigma_1 \neq 0$  and  $\Sigma_2 = 0$  and one has  $\chi$  real and  $\psi = i\psi\mathbf{n}$ , with  $\mathbf{n}$  a real unit vector. The gap reads

$$\Delta_{\pm}(\mathbf{k}) = \sqrt{(|\chi|^2 + |\psi|^2) - |\psi \cdot \hat{\mathbf{k}}|^2 \pm \sqrt{|\Sigma_1|^2 - |\Sigma_1 \cdot \hat{\mathbf{k}}|^2}}, \quad (24)$$

Choosing  $\mathbf{n} = (1, 0, 0)$  the gap then reads

$$\Delta_{\pm}^{\text{TRSB1}} \propto \left| \chi \pm \psi \sqrt{1 - \sin^2(\theta) \cos^2(\phi)} \right|. \quad (25)$$

For  $\chi = 0$  one obtains Dirac nodes at  $\theta = \pi/2, \phi = 0, \pi$  as for the nematic case. For  $0 < \chi < \psi$  one has nodal lines. These are best seen by choosing the coordinate in momentum space so to align the  $z$  direction to the nematic director (that is by choosing  $\mathbf{n} = (0, 0, 1)$ ) so that the gap reads

$$\Delta_{\pm}^{\text{TRSB1}} \propto |\chi \pm \psi \sin(\theta')|, \quad (26)$$

with  $\theta'$  the polar angle with respect to the  $x$  axis. It is then clear that the Dirac point at  $\chi = 0$  evolves in a circle.

#### TRSB 2 state

Finally we now address the character on the Fermi surface of the gap in the TRSB 2 phase, where both  $\Sigma_1$  and  $\Sigma_2$  are non-zero but with  $\Sigma_2$  not maximal. In this case one can in general write  $\psi = (\cos(\alpha/2), i \sin(\alpha/2), 0)$  and take  $\chi$  real. The gap function in this case is not particularly enlightening. Nevertheless, one can show that for  $0 < \chi < \psi$  in general one has 2 Weyl points of topological charge  $C = 1$  in the north hemisphere and 2 Weyl points of topological charge  $C = -1$  negative in the south hemisphere. As in the purely chiral state the  $\chi$  component moves the position of the Weyl points toward the equator and at  $\chi = \psi$  they merge and split, so that for  $\chi > \psi$  the state is gapped.

### Microscopic Theory of Superconductivity in $\text{Bi}_2\text{Se}_3$

In the main text we studied superconductivity in the odd parity channel for a  $\text{SO}(3)$  Dirac Hamiltonian and we referred to  $\text{Bi}_2\text{Se}_3$  as a possible material system. The  $\text{Bi}_2\text{Se}_3$  family is well described by the 3D massive Dirac equation Eq. (1) that, with the construction of the Dirac matrices in terms of spin  $\mathbf{s}$  and  $p_z$  orbital  $\sigma$  Pauli matrices given in Table I, can be casted in the form of a Dirac Hamiltonian. The actual point group of the material is  $D_{3d}$  and we now specify to this case.

We now consider the full interacting problem described by purely interlayer interaction, since it is assumed that they play a major role. We go a step beyond the purely local interaction discussed in Ref. [22] and extend the attraction

to nearest neighbors. In the Cooper channel the interaction reads

$$H_{\text{int}} = -\frac{1}{2} \sum_{i \neq j} \sum_{\mathbf{k}, \mathbf{k}'; s, s'} V(\mathbf{k} - \mathbf{k}') c_{\mathbf{k}, i, s}^\dagger c_{-\mathbf{k}, j, s'}^\dagger c_{-\mathbf{k}', j, s'} c_{\mathbf{k}', i, s}, \quad (27)$$

with  $V(\mathbf{q})$  the Fourier transform of the interaction potential. A detailed microscopic description of the nearest neighbor interaction in  $\text{Bi}_2\text{Se}_3$  is beyond the scope of the present work and we simply assume that an expansion at lowest order in  $\mathbf{q} = \mathbf{k} - \mathbf{k}'$  can be done. We take into account the anisotropy along the  $z$ -direction typical of the material by splitting the momentum as  $\mathbf{k} = (\mathbf{k}_\parallel, k_z)$  and introducing effective length scales  $a$  and  $a_z$  on order of the lattice constants. Defining  $\mathbf{k} = (\mathbf{k}_\parallel, k_z)$  the interaction reads

$$V(\mathbf{k}, \mathbf{k}') = \frac{V}{2} \left( 1 + a^2 \mathbf{k}_\parallel \cdot \mathbf{k}'_\parallel + a_z^2 k_z k'_z \right). \quad (28)$$

These terms can involve only vectorial representations and tends to increase the strength of channel interaction. The next step consists in expanding the interaction in irreducible representations of the point group  $D_{3d}$ . When  $\text{SO}(3)$  is broken down to  $D_{3d}$  the vector order parameter splits as  $\psi \rightarrow (\psi_\parallel, \psi_z)$  and we can define the following basis functions

$$\begin{aligned} \Gamma_x^1(\mathbf{k}) &= -i\gamma^5 \gamma^2 k_z, & \Gamma_x^2(\mathbf{k}) &= -i\gamma^5 \gamma^3 k_y, \\ \Gamma_y^1(\mathbf{k}) &= -i\gamma^5 \gamma^3 k_x, & \Gamma_y^2(\mathbf{k}) &= -i\gamma^5 \gamma^1 k_z, \\ \Gamma_z(\mathbf{k}) &= -i\gamma^5 (\gamma^1 k_y - \gamma^2 k_x), \end{aligned} \quad (29)$$

where  $\Gamma_x^{1,2}$  and  $\Gamma_y^{1,2}$  belong to  $E_u$  and  $\Gamma_z$  belongs to  $A_{2u}$ . Following [1] and focusing on the odd-parity sector we write the gap matrix as

$$\hat{\Delta} = \chi \gamma^5 + \boldsymbol{\psi} \cdot \boldsymbol{\gamma} + a \psi_z F_y + \psi_x (a_z F_x^1 - a F_x^2) + \psi_y (a F_y^1 - a_z F_y^2), \quad (30)$$

with both the pseudo-scalar  $\chi$  and the vector  $\boldsymbol{\psi}$  order parameters. We see that the extra terms contains the contraction of the momentum with the pseudo-vector  $\gamma^5 \boldsymbol{\gamma}$ , that is the possible odd-parity term involving the momentum only allowed by symmetry, as explained in the next section. Setting the chemical potential in the conduction band,  $\mu > m$ , upon projecting onto the conduction band [33], one obtains the gap matrix

$$\Delta_{\mathbf{k}} = \chi \tilde{\mathbf{k}} \cdot \tilde{\mathbf{s}} + \boldsymbol{\psi} \times \tilde{\mathbf{k}} \cdot \tilde{\mathbf{s}} (1 + \mu a/v) \quad (31)$$

for the isotropic case  $a = a_z$ . For the anisotropic case  $a \neq a_z$ , the projection of the basis functions Eq. (29) onto the conduction band produces the basis function introduced in Ref. [36], and by introducing the parameters  $\lambda = (1 + \mu a/v)$  and  $\lambda_z = (1 + \mu a_z/v_z)$  the gap matrix reads

$$\hat{\Delta} = \chi \tilde{\mathbf{k}} \cdot \tilde{\mathbf{s}} + \lambda \psi_z (\tilde{s}_x \tilde{k}_y - \tilde{s}_y \tilde{k}_x) + \psi_x (\lambda_z \tilde{s}_x \tilde{k}_z - \lambda \tilde{s}_z \tilde{k}_y) + \psi_y (\lambda \tilde{s}_z \tilde{k}_x - \lambda_z \tilde{s}_x \tilde{k}_z), \quad (32)$$

where the momentum has been rescaled as  $\tilde{\mathbf{k}} = (vk_x, vk_y, v_z k_z)/\mu$ . We see that the nearest neighbor interaction rescales the momentum only of the vector channel.

We now consider the role of magnetic impurities. In the normal phase Nb-doped  $\text{Bi}_2\text{Se}_3$  is found to be paramagnetic [14], so that we do not consider direct ferromagnetic coupling between the magnetic dopants. Assuming that the dopants couple in the same way to the spin of the two orbitals, the Zeeman coupling reads

$$H_Z = - \sum_i J_i \int d\mathbf{r} s_i(\mathbf{r}) m_i(\mathbf{r}), \quad (33)$$

where  $\mathbf{m}(\mathbf{r})$  is the magnetic moment density of the dopants,  $\mathbf{s}_{s,s'}(\mathbf{r}) = \sum_i c_{i,s}^\dagger(\mathbf{r}) c_{s',i}(\mathbf{r}) \mathbf{s}_{s,s'}$  is the electron spin operator, and  $J_x = J_y = J \neq J_z$  are the anisotropic Zeeman coupling constants. The spin operator  $\mathbf{s} = (s_x, s_y, s_z)$  does not transform as a pseudovector according to the transformation rules of  $\text{SO}(3)$  dictated by the representations of the  $\gamma$ -matrices in Tab. I. Indeed, it is evident from Tab. I that it is constructed with the components of  $\mathbf{S}_\parallel \equiv \gamma^5 \boldsymbol{\gamma}$  and  $\mathbf{S}_\perp \equiv \gamma^0 \gamma^5 \boldsymbol{\gamma}$ , which represent generalized spin operator of the bonding and anti-bonding configurations of the two orbitals. Considering only the  $\mathbf{q} = 0$  component of the magnetization we can then write the Zeeman coupling as

$$H_Z = -JS_\parallel^1 M^1 - JS_\parallel^2 M^2 - J_z S_\perp^3 M^3. \quad (34)$$

	$\gamma^0$	$\gamma^5$	$\gamma^0\gamma^5$	$\vec{\gamma}$	$\gamma^0\vec{\gamma}$	$\gamma^0\gamma^5\vec{\gamma}$	$\gamma^5\vec{\gamma}$
Fu model	$\sigma_x$	$\sigma_y s_z$	$\sigma_z s_z$	$(-\sigma_y s_y, \sigma_y s_x, \sigma_z)$	$(\sigma_z s_y, -\sigma_z s_x, \sigma_y)$	$(\sigma_x s_x, \sigma_x s_y, s_z)$	$(s_x, s_y, \sigma_x s_z)$
I	+	-	-	-	-	+	+
T	+	+	-	+	-	-	-
C	+	+	-	+	-	-	-
$M_x$	+	-	-	(-, +, +)	(-, +, +)	(+, -, -)	(+, -, -)

TABLE I: Classification of Dirac algebra matrices, their realization in the Fu model and their symmetry properties. I stands for inversion symmetry, T for time-reversal symmetry, C for charge conjugation, and  $M_x$  is the mirror about the  $yz$  plane. From these, there are a pseudo-scalar  $\gamma^0\gamma^5$  and a vector  $\gamma^0\gamma^i$  that are odd under parity and, combined with the momentum, give rise to even parity pairing, thus only correcting the momentum-independent even-parity channels. The remaining two pseudo-vectors  $\gamma^0\gamma^i$  and  $\gamma^0\gamma^5\gamma^i$  are even under parity and combined with the momentum they can give odd parity pairing.

This coupling breaks the SO(3) symmetry by mixing the two operators  $\mathbf{S}_{\parallel}$  and  $\mathbf{S}_{\perp}$ . By projecting the Zeeman term onto the eigenstates of the conduction band at  $\mathbf{k} = 0$  one has  $H_Z = -\tilde{\mathbf{s}} \cdot \hat{J} \cdot \mathbf{M}$ , with  $\hat{J} = \text{diag}(J, J, J_z)$ , where the projection of both  $\mathbf{S}_i$  generalized spin operator gives the spin of the conduction band  $\tilde{\mathbf{s}}$ . For  $\mathbf{k}$  on the Fermi surface one has the mapping

$$S_{\parallel}^i \rightarrow \tilde{s}_i - \frac{\mu}{m + \mu} \tilde{k}_i \tilde{\mathbf{k}} \cdot \tilde{\mathbf{s}}, \quad S_{\perp}^i \rightarrow \frac{m}{\mu} \tilde{s}_i + \frac{\mu}{m + \mu} \tilde{k}_i \tilde{\mathbf{k}} \cdot \tilde{\mathbf{s}}. \quad (35)$$

### Derivation of the Ginzburg - Landau free energy

We now derive the Ginzburg-Landau free energy starting from the microscopic model. For simplicity we refer to the isotropic case  $a_z = a$ ,  $v_z = v$ , but keep the anisotropy in the Zeeman term. The inclusion of the Zeeman coupling to the Bogolyubov-deGennes Hamiltonian in the Nambu basis  $\Psi_{\mathbf{k}} = (\mathbf{c}_{\mathbf{k}}, \mathcal{T}\mathbf{c}_{\mathbf{k}})^T$  results in the addition of a term  $H_Z$  with equal sign for electrons and holes. We can now integrate away the fermionic degrees of freedom and obtain a non-linear functional for the order parameters,

$$\mathcal{S} = \int_0^{\beta} d\tau \frac{1}{V} \text{Tr} [\hat{\Delta}^{\dagger} \hat{\Delta}] - \frac{1}{\beta} \text{Tr} \ln(\mathcal{G}_0^{-1} - \Sigma), \quad (36)$$

with  $-\mathcal{G}_0^{-1} = \partial_{\tau} + (H_0 - \mu)\tau_z$  and  $\Sigma = \tau^+ \hat{\Delta} + \tau_z H_Z$ , and the trace is over all the degrees of freedom,  $\text{Tr} \equiv T \sum_{\omega} \int d\mathbf{k}$ . As usual, the microscopic GL theory is obtained by expanding the non-linear action in powers of the fields,

$$-\frac{1}{\beta} \text{Tr} \ln(-\mathcal{G}_0^{-1} + \Sigma) = -\frac{1}{\beta} \text{Tr} \ln(-\mathcal{G}_0^{-1}) - \frac{1}{\beta} \sum_{n=1}^{\infty} \frac{1}{n} \text{Tr}(\mathcal{G}_0 \Sigma)^n. \quad (37)$$

We first focus on the superconducting order parameter and set  $J = 0$ . The second order terms are given by  $\langle \Delta_{\mathbf{k}} \Delta_{\mathbf{k}}^{\dagger} \rangle_{(2)}$  and the fourth order coefficient are determined by the fourth order averages  $\langle \Delta_{\mathbf{k}} \Delta_{\mathbf{k}}^{\dagger} \Delta_{\mathbf{k}} \Delta_{\mathbf{k}}^{\dagger} \rangle_{(4)}$ , where  $\langle \dots \rangle_{(2)} = T \sum_{\omega_n} \int \frac{d\mathbf{k}}{(2\pi)^3} G_+ G_- \text{Tr}[\dots]$  and  $\langle \dots \rangle_{(4)} = \frac{T}{2} \sum_{\omega_n} \int \frac{d\mathbf{k}}{(2\pi)^3} G_+^2 G_-^2 \text{Tr}[\dots]$ , with the unperturbed Green's function given by  $G_{\pm} = (i\omega_n \mp \xi_{\mathbf{k}})^{-1}$ ,  $\xi_{\mathbf{k}} = \epsilon_{\mathbf{k}} - \mu$  and  $\epsilon_{\mathbf{k}} = \sqrt{v^2 \mathbf{k}^2 + m^2}$  is the dispersion of the conduction band.

The matrix which describes the gap function in spin space for the two component representation  $\psi_{\parallel}$  is

$$\Delta_{\mathbf{k}} = \chi \tilde{\mathbf{k}} \cdot \mathbf{s} + \sum_{i=x,y} \psi_i \mathbf{d}_i \cdot \mathbf{s}, \quad (38)$$

with  $\mathbf{d}_x = (0, -\tilde{k}_z, \tilde{k}_y)\lambda$ ,  $\mathbf{d}_y = (\tilde{k}_z, 0, -\tilde{k}_x)\lambda$ . The coefficients of the GL free energy of the second order couplings are given by

$$a_1 = \frac{1}{V} - \chi_0(T) \langle \tilde{k}^2 \rangle_{\text{FS}}, \quad (39)$$

$$a_2^{ij} = \frac{1}{V} - \chi_0(T) \langle \mathbf{d}_i \cdot \mathbf{d}_j \rangle_{\text{FS}} (1 + \mu a/v)^2 \quad (40)$$

where  $\chi_0(T) = N(\epsilon_F) \int d\epsilon \tanh(\epsilon/2T)/\epsilon$ ,  $N(\epsilon_F) = \mu^2 \sqrt{1 - m^2/\mu^2}/(2\pi^2 v^3)$  is the density of states at the Fermi level,  $\langle \dots \rangle_{\text{FS}} = \int \frac{d\mathbf{k}}{(2\pi)^3} \delta(\epsilon_{\mathbf{k}} - \mu) \dots$  stands for Fermi surface average, and the coupling of the components vector order

parameter are diagonal,  $a_2^{ij} = \delta_{ij}a_2$ . The second order coefficients allows us to determine the critical temperature of the independent channels, and we find

$$\frac{1}{V} = \chi_0(T_\chi)(1 - m^2/\mu^2), \quad (41)$$

$$\frac{1}{V} = \frac{2}{3}(1 + \mu a/v)^2 \chi_0(T_\psi)(1 - m^2/\mu^2). \quad (42)$$

It becomes clear that nearest neighbor interactions can increase the critical temperature of the vector order parameter, so that it is reasonable to consider both at the same time and study the coupled theory.

The coefficient  $a_3$  of the second order term in  $\mathbf{M}$  contains two terms: i) the susceptibility of the free magnetic moment, and ii) the term coming from the second order expansion Eq. (37), and it can be approximated to a positive constant.

The higher order terms in the GL free energy are obtained by the higher order expansion of the functional Eq. (37). The third order term gives the coupling between the magnetization and the pseudo-vector  $\Sigma_1$  and  $\Sigma_2$  introduced in the main text. The anisotropic Zeeman breaks the SO(3) symmetry down to the  $D_{3d}$  point group. By writing the third order coupling as

$$F^{(3)} = ic_1 \mathbf{M}_\parallel \cdot (\chi \psi_\parallel^* - \chi^* \psi_\parallel) + ic_2^z M_z \psi_\parallel \times \psi_\parallel^* \quad (43)$$

the values of the coupling for the in-plane  $c_2$  and out-of-plane  $c_2^z$  components of the magnetization reads

$$c_2^z = \frac{2}{3} J_z (1 - m^2/\mu^2) \mu \kappa, \quad (44)$$

$$c_1 = \frac{4}{3} J (1 - m^2/\mu^2) \mu \kappa. \quad (45)$$

The coefficient of the fourth order terms for the isotropic case become

$$b_1 = \kappa(1 - m^2/\mu^2)^2, \quad b_2 = \frac{8}{15} \lambda^4 b_1, \quad b_2' = \frac{4}{15} \lambda^4 b_1, \quad d_1 = \frac{4}{3} \lambda^2 b_1, \quad d_2 = \frac{2}{3} \lambda^2 b_1 \quad (46)$$

with  $\kappa = N(\epsilon_F)7\zeta(3)/(8(\pi T_c)^2)$ . It follows that the phase diagram for the anisotropic case governed by the couplings  $J$  and  $J_z$  is qualitatively similar to the one in the main text.

### Parametrization of the vector $\psi$

We now present a parametrization of the vector order parameter that allows to simplify the analysis of the free energy of the coupled system. The order parameter  $\psi = (\psi_x, \psi_y, \psi_z)$  is described by three complex or six real degrees of freedom. If we write  $\psi = \psi_0(\mathbf{u} + i\mathbf{v})$  with  $u^2 + v^2 = 1$  with  $u = |\mathbf{u}|$  and  $v = |\mathbf{v}|$ , the different terms in the free energy take the form

$$\psi \cdot \psi^* = \psi_0^2, \quad (47)$$

$$\psi \times \psi^* = -i\psi_0^2 2\mathbf{u} \times \mathbf{v} \quad (48)$$

$$\psi \cdot \psi = \psi_0^2(u^2 - v^2 + 2i\mathbf{u} \cdot \mathbf{v}) = \psi_0^2 \sqrt{1 - (2\mathbf{u} \times \mathbf{v})^2} e^{i\phi} \quad (49)$$

$$\phi = \arctan \frac{2\mathbf{u} \cdot \mathbf{v}}{u^2 - v^2} \quad (50)$$

This motivates the parametrization  $u = \cos \alpha/2$ ,  $v = \sin \alpha/2$ ,  $0 \leq \alpha \leq \pi$  and

$$X = 2\mathbf{u} \cdot \mathbf{v} = 2uv \cos \theta = \sin \alpha \cos \theta \quad (51)$$

$$Y = 2|\mathbf{u} \times \mathbf{v}| = 2uv \sin \theta = \sin \alpha \sin \theta \quad (52)$$

$$Z = u^2 - v^2 = \cos \alpha \quad (53)$$

where the variables are so labeled due to the resemblance to spherical coordinates.  $\theta$  is defined as the relative angle between  $\mathbf{u}$  and  $\mathbf{v}$ . When we consider the coupling to the magnetization, the absolute directions of  $\mathbf{u}$  and  $\mathbf{v}$  need to be defined. The simplest way is to define  $\phi'$  and  $\theta'$  as the absolute angles in spherical coordinates of the unit vector

$\mathbf{u} \times \mathbf{v}/uv$  and  $\gamma'$  as the absolute azimuthal angle of  $\mathbf{u}$  with respect to the axis  $\mathbf{u} \times \mathbf{v}/uv$ . The six real variables that parametrize  $\boldsymbol{\psi}$  are therefore  $\psi, \alpha, \theta, \phi', \theta', \gamma'$ .

The two TRSB phases discussed in the text can be distinguished by the way rotation symmetry is broken in each of them. In the TRSB 1 phase, where only  $\Sigma_1$  is finite, the ground state remains invariant under  $\text{SO}(2)$  rotations around the  $\Sigma_1$  axis. In the phases where  $\Sigma_2$  is finite, assuming that  $\Sigma_2$  points in the  $z$  direction, the vector order parameter is given by  $\boldsymbol{\psi} = \psi_0[u(\cos \gamma', \sin \gamma', 0) + iv(\cos(\gamma' - \theta), \sin(\gamma' - \theta), 0)]$ . In the fully chiral phase where  $u = v = 1/\sqrt{2}$  and  $\theta = \pi/2$ , we have  $\boldsymbol{\psi} = \psi_0 e^{i\gamma'}(1, i, 0)/\sqrt{2}$ , so that a rotation around the  $\Sigma_2$  axis corresponds to a shift in  $\gamma'$ , which becomes a phase shift of  $\boldsymbol{\psi}$ . This phase shift is not a pure gauge because of the presence of  $\chi$ , but if we shift the phase of  $\chi$  by the same amount, this operation becomes a true symmetry of the fully chiral phase. Indeed, both  $\Sigma_1$  and  $\Sigma_2$  remain invariant under this mixed gauge-rotational symmetry. Finally, this symmetry is broken in the hybrid phase TRSB 2, where  $u \neq v$ , and no residual rotation symmetry remains.

### Hybrid TRSB solution of $F_{\chi, \psi}$

We now consider in detail the coupling between the scalar and the vector phase in the case the  $\text{SO}(3)$  is broken down to  $D_{3d}$ . The GL free energy is given by

$$F = F_\chi + F_\psi + F_{\chi, \psi}. \quad (54)$$

The phase diagram as a function of temperature and interaction parameters  $b'_2, d_1$ , and  $d_2$  that admits three possible phases: i) the  $A_{1u}$  phase, where only the scalar  $\chi$  condenses,  $\chi = \chi_A$  and  $\boldsymbol{\psi} = 0$ , ii) a nematic time reversal invariant phase with  $\chi = \chi_N$  and  $\boldsymbol{\psi} = \boldsymbol{\psi}_N$  real, and iii) a hybrid TRSB phase with  $\chi = \chi_h$  and  $\boldsymbol{\psi} = \boldsymbol{\psi}_h$  complex. We define  $T_A$  the condensation temperature of the scalar  $A_{1u}$  phase and  $T_E$  the condensation temperature of the two-component  $E_u$  and assume the system to be at  $T < T_E$ .

Employing the parametrization introduced in the previous section for the vector  $\boldsymbol{\psi}$  and setting  $\chi = \chi_0 e^{i\gamma}$  the free energy is written as

$$F = a_1 \chi_0^2 + b_1 \chi_0^4 + a_2 \psi_0^2 + (b_2 + b'_2 Y^2) \psi_0^4 + [d_1 + 2d_2 - 2d_2 \sqrt{1 - Y^2} \cos(\phi - 2\gamma)] \chi_0^2 \psi_0^2 \quad (55)$$

with  $\phi = \arctan X/Z$ . Note that  $\phi$  and  $Y$  can be taken as independent variables since they also parametrize the full sphere, so that we can minimize independently for  $Y$  and  $\phi$  without a constraint. Since the parametrization of  $\boldsymbol{\psi}$  contains 4 real parameters, it does contain arbitrary changes of the overall phase (i.e. gauge transformations), so that in principle we can assume  $\chi$  to be real and  $\gamma = 0, \pi$ . However, when studying vortices or configurations where the phase changes in real space we need to keep  $\gamma$ .

The usefulness of this parametrization when  $\gamma = 0$  is that  $\phi$  can always be minimized independently, since it is clear that regardless of the rest of the parameters one obtains a lower energy by setting  $\phi = 0, \pi$  for positive or negative  $d_2$ . This corresponds to having  $X/Z = \tan \alpha \cos \theta = 0$ , which gives two options. First, if  $\alpha = 0, \pi$ , then either  $u$  or  $v$  is zero, which is a nematic solution with the same phase as  $\chi$ , hence no TRSB phase. Second, if  $\theta = \pm\pi/2$  then  $\mathbf{u}$  and  $\mathbf{v}$  are orthogonal and this is a TRSB phase, where the relative weight of  $u$  and  $v$  is obtained from minimizing with respect to  $Y = \sin \alpha$  (for finite alpha since otherwise we are in the previous solution).

The minimization with respect to  $Y$  now has the following options. If  $b'_2 > 0$  and  $d_2 > 0$ , then we always get  $Y = 0$  and a nematic phase, since both terms that contain  $Y$  want it to be as small as possible. If  $b'_2 < 0$  and  $d_2 > 0$  then there is a competition between  $b'_2$  which favors the chiral solution and  $d_2$  which favors the nematic solution. The value of  $Y$  is obtained from

$$2b'_2 \psi_h^4 Y + 2d_2 Y \psi_h^2 \chi_h^2 / \sqrt{1 - Y^2} = 0 \quad (56)$$

which gives the solution

$$Y = \sqrt{1 - \frac{d_2^2 \chi_h^4}{(b'_2)^2 \psi_h^4}}, \quad (57)$$

which interpolates between nematic and the standard chiral as  $Y$  goes from 0 to 1. Finally, if  $b'_2 < 0$  and  $d_2 < 0$  one has  $Y = 0$  and  $\phi - 2\gamma = \pi$ , that corresponds to a solution in which  $\boldsymbol{\psi}$  is real and  $\chi = -i\chi_0$ .